Journal Pre-proofs

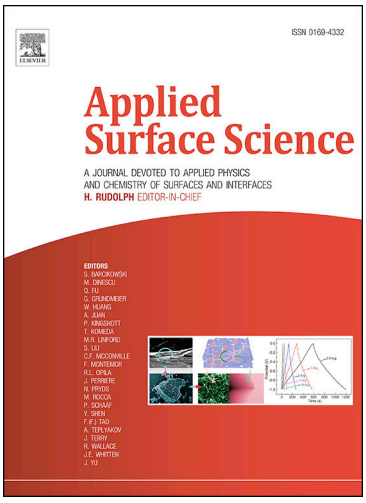

Full Length Article

Nickel ion extracellular uptake by the phototrophic bacterium *Rhodobacter sphaeroides*: new insights from Langmuir modelling and X-ray photoelectron spectroscopic analysis

Daniela Chirizzi, Disma Mastrogiacomo, Paola Semeraro, Francesco Milano, Anna Rita De Bartolomeo, Massimo Trotta, Ludovico Valli, Livia Giotta, Maria Rachele Guascito

PII: S0169-4332(22)00938-2
DOI: https://doi.org/10.1016/j.apsusc.2022.153385
Reference: APSUSC 153385

To appear in: *Applied Surface Science*

Received Date: 18 January 2022
Revised Date: 7 April 2022
Accepted Date: 10 April 2022

Please cite this article as: D. Chirizzi, D. Mastrogiacomo, P. Semeraro, F. Milano, A. Rita De Bartolomeo, M. Trotta, L. Valli, L. Giotta, M. Rachele Guascito, Nickel ion extracellular uptake by the phototrophic bacterium *Rhodobacter sphaeroides*: new insights from Langmuir modelling and X-ray photoelectron spectroscopic analysis, *Applied Surface Science* (2022), doi: https://doi.org/10.1016/j.apsusc.2022.153385

Nickel ion extracellular uptake by the phototrophic bacterium *Rhodobacter sphaeroides*: new insights from Langmuir modelling and X-ray photoelectron spectroscopic analysis

Daniela Chirizzi[1], Disma Mastrogiacomo[2], Paola Semeraro[2,3], Francesco Milano[4], Anna Rita De Bartolomeo[2], Massimo Trotta[5], Ludovico Valli[2,3], Livia Giotta[2,3,], and Maria Rachele Guascito[2,3]*

[1] Istituto Zooprofilattico Sperimentale della Puglia e della Basilicata (IZS_PB), Via Manfredonia 20, I-71100 Foggia, Italy

[2] Dipartimento di Scienze e Tecnologie Biologiche e Ambientali, Università del Salento, S.P. Lecce-Monteroni, I-73100 Lecce, Italy

[3]Consorzio Interuniversitario Nazionale per la Scienza e Tecnologia dei Materiali (INSTM), Unità di Lecce, S.P. Lecce-Monteroni, I-73100 Lecce, Italy

[4] Istituto di Scienza delle Produzioni Alimentari (ISPA), Consiglio Nazionale delle Ricerche (CNR), UOS Lecce, S.P. Lecce-Monteroni, I-73100 Lecce, Italy

[5] Istituto per i processi Chimico-Fisici (IPCF), Consiglio Nazionale delle Ricerche (CNR), UOS Bari, Via Orabona, 4, I-70126 Bari, Italy

*corresponding author: livia.giotta@unisalento.it

KEYWORDS: Nickel(II), biosorption, bioremediation, lipopolysaccharide, outer membrane, X-ray photoelectron spectroscopy, Langmuir isotherm.

ABSTRACT

The presence of anionic functional groups on the surface of microbial cells makes the bacterial biomass very attractive as metal cation removal tool for environmental bioremediation. To go insight to the heavy metal sorption abilities of Gram-negative bacteria, we characterized the extracellular uptake of Ni^{2+} ions by the phototrophic bacterium *Rhodobacter sphaeroides*, whose ability to sequester toxic metal ions has been widely documented. The sorption process proved to be well described by the Langmuir model, suggesting that the cell envelope behaves as an ideal adsorbent surface, showing a layer of chemically equivalent binding sites with high affinity for Ni^{2+}. X-ray photoelectron spectroscopic data reveal that, at binding site saturation, Ni^{2+} ions fully displace alkaline ions from the bacterial surface, while they are unable to displace Ca^{2+} and Mg^{2+} from their tight binding sites. The analysis of carbon, nitrogen and oxygen speciation, as arisen from high resolution spectra fitting, highlights that the Ni^{2+}/K^{+} cation exchange affects the surface distribution of main chemical components, with increased contribution by peptides and phosphatidylcholines. A role of Ni^{2+} ions in favoring the stacking and/or packing of lipopolysaccharide sugar chains by interaction with carboxylate groups is proposed and discussed.

1. INTRODUCTION

The pollution by heavy metals represents a major concern for the modern society since most of these chemicals are extremely dangerous. Their release in the environment has increased in the last decades due to industrialization and urbanization, favoring the exposure of people at doses capable of generating adverse reactions[1]. Contamination by toxic heavy metals can occur in different environmental compartments such as soils, sediments, atmosphere, groundwaters, rivers, lakes and seas[2]. Unlike organic pollutants, metals cannot be degraded and, being persistent, may undergo bio-magnification moving up the food chain, particularly in aquatic environments[3]. Toxic metals can enter the human body by ingestion of contaminated water and food, via the respiratory tract or by skin contact. Acute, chronic or sub-chronic adverse effects can arise from exposure to heavy metals, most of which exhibit neurotoxicity, carcinogenicity, mutagenicity and teratogenicity[4,5].

Nickel pollution of aquatic environments is mainly due to domestic wastewater effluents and to sewer water by metal smelters[6]. Its toxicity arises mostly from its ability to interfere with the metabolism of essential divalent ions, such as Fe^{2+}, Mn^{2+}, Cu^{2+}, Mg^{2+} and Ca^{2+} by replacing them in enzymes or carrier proteins. Adverse effects due to nickel exposure include dermatitis, respiratory diseases, respiratory carcinogenicity and reproductive toxicity[7].

Beside the enhancement of sensing technology[8], the design of remediation strategies aimed at recovering hazardous metals from the environment represents therefore a big challenge for the modern society. Big efforts have been made in the last years in order to exploit the potential of living organisms, such as plants, algae, fungi and bacteria, in promoting the detoxification of environmental matrices, particularly soils and waters. The so-called bioremediation technology presents indeed a number of advantages with respect to conventional techniques, including

cheapness, versatility, selectivity and low environmental impact[9–11]. A number of biosorbents have been tested for their employment in heavy metal removal from contaminated waters[12,13]. Biosorbents may consist either of whole cells (both living[14] and non-living[15]), or by their components, which can be properly treated and/or modified in order to enhance removal capacity[16]. Waste products arising from either agriculture, forestry or food industry have also been employed[17,18].

The purple bacterium *Rhodobacter (R.) sphaeroides* has been investigated in the last years for its ability to tolerate and immobilize heavy metal ions[19–21]. Its employment as a biosorbent in bioremediation processes aimed at metal ion removal and recovery has been proposed based on the physico-chemical characterization of microbial cell/heavy metal interaction. A major role of extracellular uptake in promoting the removal of Ni^{2+} and Co^{2+} ions from aqueous solutions has been demonstrated[22] and the chemical nature of functional groups mainly involved in Ni^{2+} binding has been enlightened by a molecular spectroscopic approach[23]. In particular, Ni^{2+} proved to establish coordinative bonds with carboxylate moieties on the bacterial surface of *R. sphaeroides* competing with protons[23], thus suggesting the effectiveness of acidic wash for the recovery process. Nickel divalent cation is considered a borderline acid in the hard and soft acid-base (HSAB) classification based on Pearson theory[24]. Therefore, its interaction with the hard basis COO^- is expected to show both covalent and electrostatic character. Further anionic groups with hard bases characteristics, such as sulphonates and phosphonates, might also be involved in the binding, as well as aminoacid residues, such as histidine, whose affinity with Ni^{2+} is well estabished. Moreover, competition with other metal cations is expected to affect the overall nickel uptake capacity by bacterial biomass.

With this work we intend to further characterize the extracellular Ni^{2+} uptake by *R. sphaeroides* cells using both a standard thermodynamic approach based on Langmuir adsorption isotherm modelling and a surface-sensitive spectroscopic approach based on X-ray Photoelectron Spectroscopy (XPS).

The Langmuir model[25] is often employed in order to evaluate the sorption performances of different adsorbent matrices. It is based on the presence of a single layer of equivalent binding sites on the surface of the adsorbent and on the absence of any interaction between bound sorbate molecules. The parameters that can be obtained by applying the Langmuir model are usually referred as q_{max} (the highest monolayer coverage) and K_L (Langmuir constant) , which are related to the total amount of binding sites lying on the adsorbent surface and to the affinity of the sorbate for the binding sites respectively[26,27]. The bacterial cell does not present exactly the features of the ideal adsorbent surface described by the Langmuir model[28], since the binding sites lying on the microbial envelope are not chemically equivalent and in addition intracellular uptake mechanisms might contribute to the overall immobilization ability. Nevertheless, the Langmuir isotherm proved to describe quite well a wide range of biological adsorbent matrices[26,29–31] and its extensive application in the scientific community made it the best model to adopt in order to compare the performances of new adsorbents with those already described and characterized.

On the other side, XPS has been employed for the characterization of bacterial cells, offering information about the elemental composition of the surface of a number of microorganisms[32–34]. The influence of different growth conditions and pH on the atomic ratios of elements on the surface of microbial cells has been also reported[35–37]. Much effort has been made for correlating N/P, O/C, and N/C ratios to different properties of bacterial cells, such as electrophoretic mobility[34,38], hydrophobicity[39,40], and polysaccharide content[41]. All these

investigations have shown that XPS technique is able to detect with high sensitivity the chemical differences of the outermost layer of microbial cell, arising from different environmental conditions and/or different genotypes. Distinct mutants of the same species have been even discriminated[41], since in these cases the mutation induced a chemical modification of the surface structure. XPS characterization has been often combined with FTIR analysis[39,41–43], in order to correlate macro-element ratios to specific functional groups. Hence it appeared interesting to integrate the infrared investigation already performed on *R. sphaeroides*/Ni^{2+} interaction[23] with an XPS study. On the other hand, despite the high number of investigations reporting the employment of XPS in microbial cell characterization, the application of this technique for the comprehension of bacterial surface/heavy metal cation interaction has been reported only in few cases relevant to thermoacidophilic archaea[44], anaerobic ammonium-oxidizing bacteria[43] and bacteria belonging to the genera *Bacillus*[37,45,46], *Lysinibacillus*[47] and *Enterococcus*[48]. To the best of our knowledge, only two reports have recently appeared about the employment of XPS for investigating Ni^{2+} binding to bacterial surfaces[46,49]. To further assess the potentialities of XPS technique in this intriguing investigation field, we have therefore deeply analyzed the surface of *R. sphaeroides* cells exposed to Ni^{2+} ions, crossing the results with equilibrium binding parameters arising from Langmuir modelling and previous FTIR data[23]. Valuable information about the surface chemical modification of this Gram-negative bacterium induced by nickel binding was gained, pointing out possible toxicity mechanisms triggered by heavy metal cation stress.

2. MATERIAL AND METHODS

2.1 Biomass preparation

All chemicals for biomass preparation were purchased from Sigma-Aldrich. Cells of *R. sphaeroides* strain R26.1 were gained from the German Collection of microorganisms and Cell Cultures (Deutsche Sammlung von Mikroorganismen und Zellkulturen GmbH - DSMZ number 2340). Bacterial cells were grown photoheterotrophically in 1.2 L glass bottles in the medium 27 of the DSMZ, whose pH was poised at 6.9. The microbial biomass was collected at the early stationary phase. The growth medium was separated by centrifugation and the pellet was washed three times with KCl 0.1 M at neutral pH. This treatment removes all loosely bound cations from the negatively charged microbial surface, replacing them with K^+. As pointed out by Borrok and coworkers[50], this wash does not cause the displacement of more tightly bound divalent cations such as Mg^{2+} and Ca^{2+}. The washed pellet was stored in 5 mL aliquots at -25°C until use.

Ni^{2+} uptake measurements

Ni^{2+} stock solutions were prepared dissolving $NiCl_2 \cdot 6H_2O$ (Sigma-Aldrich) in ultrapure water (ρ=18.2 MΩ·cm). Cells aliquots were thawed, washed twice with ultrapure water, and suspended to around 10^{10} CFU/mL. Suitable volumes of the resulting suspension were dried in the oven at 37°C to constant weight and the dry biomass was weighted to determine the dry biomass concentration. Aliquots of the bacterial suspensions were mixed in 10 mL tubes with proper Ni^{2+} concentration to realize different biomass/metal ratios. HEPES buffer (Sigma-Aldrich) was added to each tube at 50 mM final concentration, in order to equilibrate the pH at 6.5. Cells were let to interact with Ni^{2+} ions in a thermostatic bath at 25±1°C for 2 hours. Afterwards the bacterial biomass was separated by centrifugation at 5000 g and the supernatant was analyzed for determining the equilibrium Ni^{2+} concentration. For evaluating the sorption kinetics, aliquots were

withdrawn from the cell suspension interacting with the metal at fixed times and the biomass was again pelleted by centrifugation and analyzed.

The concentration of Ni^{2+} in the supernatants was determined by a standard colorimetric assay using the well-known nickel-specific dimethylglyoxime (DMG) ligand[51]. Alkaline and oxidative conditions were employed to prevent the precipitation of the Ni/DMG complex, thus allowing its rapid quantification by absorption visible spectrophotometry. Briefly a 2% (w/w) solution of DMG in NaOH 2N was prepared. The assay buffer was obtained mixing 4 mL of this solution with 2.5 mL of NH_3 5 N and 1 mL of potassium persulfate 2% (w/w), diluting to 25 mL with ultrapure water. A 40 µL aliquot of sample or standard was added to 1mL of the assay buffer and stirred. The color development proved to be complete after 15-20 minutes. Absorbance readings were performed at 465 nm using a Cary5000 UV-vis-NIR spectrophotometer (Agilent Technologies). Three replicates were prepared and analyzed for each sample. A calibration curve was built using suitable standard solutions and proved linear over the concentration range of interest.

The metal uptake q (mg/g), i.e. the amount of sorbate bound by the unit of sorbent phase, was determined as follows:

$$q = \frac{(C_i - C_{eq})V}{S} \quad (eq.1)$$

where C_i (mg/L) is the initial metal concentration, C_{eq} (mg/L) is the equilibrium metal concentration in the supernatant after uptake by the sorbent, V (L) is the volume of the solution and S (g) is the mass of the dry sorbent phase.

2.2 XPS measurements and data curve fitting

XPS analysis was carried out using an AXIS ULTRA DLD (Kratos Analytical) spectrometer equipped with a Al Ka (1486.6 eV) monochromatic source (line width 0.2 eV), operating at 10 kV and 15 mA (150W) and providing an X-ray spot size of approximately 1 mm × 2 mm. The pressure in the analysis chamber was tipically 3.0×10^{-9} torr. Survey and high-resolution (HR) spectra of main elements (C1s, O1s, N1s, S2p, P2p, Ni2p, Ca2p, K2p, Mg2s, Cl2p) were acquired in fixed analyzer transmission (FAT) mode, with survey spectra at pass energy of E_0 = 160 eV and energy step of 1 eV, and HR spectra at pass energy of E_0 = 20 eV and energy step of 0.1 eV. The analyzed area (700 μm × 300 μm), representing a portion of the X-ray spot area, was defined by applying the hybrid lens mode (large area mode acquisition). A careful charging effect correction was performed by means of the electron flood gun of which the AXIS spectrometer is equipped[52]. In detail, to prevent surface charge build-up, charge neutralization was accomplished with a filament current of 2.0 A, a filament bias voltage of 1.3 V, and a charge balance voltage of 3.6 V. At large area mode acquisition, the resolution for conductor Ag specifications was guaranteed on the $Ag3d_{5/2}$ peak with a full width at half maximum height (FWHM) of 0.47 eV at E_0 = 20 eV, and of 0.73 eV at E_0 = 160 eV. Instead, the resolution for insulator polyethylene terephthalate (PET) standard specifications was guaranteed on the carbon ester component peak (O=C-O), whose FWHMs were 1.0 eV at E_0= 20 eV and 1.3 eV at E_0= 160 eV. HR spectra were referenced to the C1s main component binding energy (BE) of the adventitious hydrocarbon at 285.0 eV [53]. The rationale for such choice arises from the following condiderations. C1s peak maxima, coming up from all samples and from the contamination recorded on the relevant supports, were found to be coincident with a variability of ±0.2 eV, when suitable charge neutralization and isolation from ground were accomplished. This finding supports the assumption that the contribution of C-C/C-

H due to the contamination cannot be distinguished from the C-C/C-H signal arising from the characteristic cell surface composition. In addition, we have monitored the modified Auger parameter α', i.e. the sum of the binding energy of the most intense photo-peaks and the kinetic energy of the sharpest respective Auger peaks, for carbon (C1s) and nickel ($Ni2p_{3/2}$). This internal parameter is not affected by charging effects and its variation for a specific element in different samples indicates distinct chemical states [54]. Similar α' values for C1s of cell samples and supports (adventitious contamination), reported in Table S1, confirm that all carbon chemical species associated to the most intense C1s peak are chemically equivalent. These outcomes demonstrate the reliability of the BE correction adopted in this work, based on referencing to aliphatic C1s at 285.0 eV. The modified Auger parameter α' for nickel was evaluated to identify its chemical speciation [54] in cell surfaces exposed to the metal.

Peaks were assigned based on literature data and on the NIST standard reference database[55]. Peak areas were converted to atomic percents (At%) using established procedures and the appropriate sensitivity factors (SF) to ensure the correct elemental mass balance, in the limit of our accuracy[56,57]. A homemade program (NewGoogly curve-fitting software program), kindly provided by Salvi and Castle[58], was used for XPS HR peak analysis and peak fitting. Details about this procedure have been provided in the Supplementary Information.

Samples for XPS analysis were prepared as follows: aliquots (50 µL) of cell suspensions coming from different treatements were cast on glass slides to cover an area of about 1 cm^2 and let to dry spontaneously at room temperature for at least 2 h; the resulting dry films with a surface cell concentration of approximately $6x10^9$ CFU/cm^2 were transferred in the spectrometer. The homogeneity and compactness of bacterial layers prepared with this procedure were demonstrated by the absence in the spectra of any XPS signals due to the glass substrate (Si2p and Si2s peaks).

The following bacterial samples were analysed: (1) control bacterial cells (from now on referred to as Ctrl cells), as obtained from KCl wash and not exposed to Ni^{2+}, (2) bacterial cells exposed to $NiCl_2$ 1.2 mM (referred to as Ni1.2 cells) and (3) bacterial cells exposed to $NiCl_2$ 12 mM (referred to as Ni12 cells). The incubation time for nickel treatment was 1 h and the $NiCl_2$ solution was in large excess with respect to the microbial biomass (metal/dry biomass ratio (w/w) >100), so that the initial metal concentration remained substantially constant during the interaction experiments. Before deposition, all cell samples were carefully washed twice with deionized water by centrifugation/resuspension steps, with the purpose of removing any residual salts coming from the treatments. The analysis of $NiCl_2$ as a reference compound was conducted placing the salt on a conductive double-sided copper tape. All reported atomic percentage compositions were representative of the mean values obtained with four different spots of the Ctrl, Ni1.2 and Ni12 samples. The relevant standard errors represent the variability observed between these four randomly selected different spots.

3. RESULTS AND DISCUSSION

3.1 Ni^{2+} uptake by *R. sphaeroides* biomass

R. sphaeroides biomass proved to sequester effectively Ni^{2+} ions, reaching a removal efficiency close to 100% at biomass/Ni ratios above 300 g/g (Figure 1a). The adsorption kinetics was very fast, so that the time resolution of our experimental set-up was not sufficient to detect accurately its profile (Figure 1b). Nevertheless, our data allowed assessing that the thermodynamic equilibrium between biosorbent and solution can be attained within 5 minutes, a quite short contact time, consistent with highly accessible surface binding sites and low activation energies of relevant binding reactions. This short equilibration time is in agreement with perfusion experiments

reported in a previous work[23] and makes this biosorbent extremely promising for bioremediation applications.

Metal uptake q was found to increase with sorbate equilibrium concentration (C_{eq}) until a plateau value was reached according to the Langmuir equation:

$$q = \frac{q_{max} K_L C_{eq}}{1 + K_L C_{eq}} \quad (eq.2)$$

where q_{max} is the maximum uptake capacity and K_L represents the Langmuir constant. The relevant Langmuir isotherm for Ni^{2+} biosorption by *R. sphaeroides* is depicted in Figure 2c, while Figure 2d shows the linear plot arising from the linearized Langmuir equation:

$$\frac{C_{eq}}{q} = \frac{1}{q_{max} K_L} + \frac{1}{q_{max}} C_{eq} \quad (eq.3).$$

q_{max} and K_L values were obtained from the linear plot fitting parameters and reported in Table 1, together with analogous data available in the literature for other bacterial adsorbents. Relevant experimental conditions, such as dehydration temperature and state of the bacterial biomass (dried or live non growing) are also marked. The high R^2 value (0.995) demonstrated the very good adequacy of the Langmuir model for the biosorption process considered in this work. A lower R^2 value (0.963) was instead obtained in the case of the Freundlich model, which therefore was not considered here.

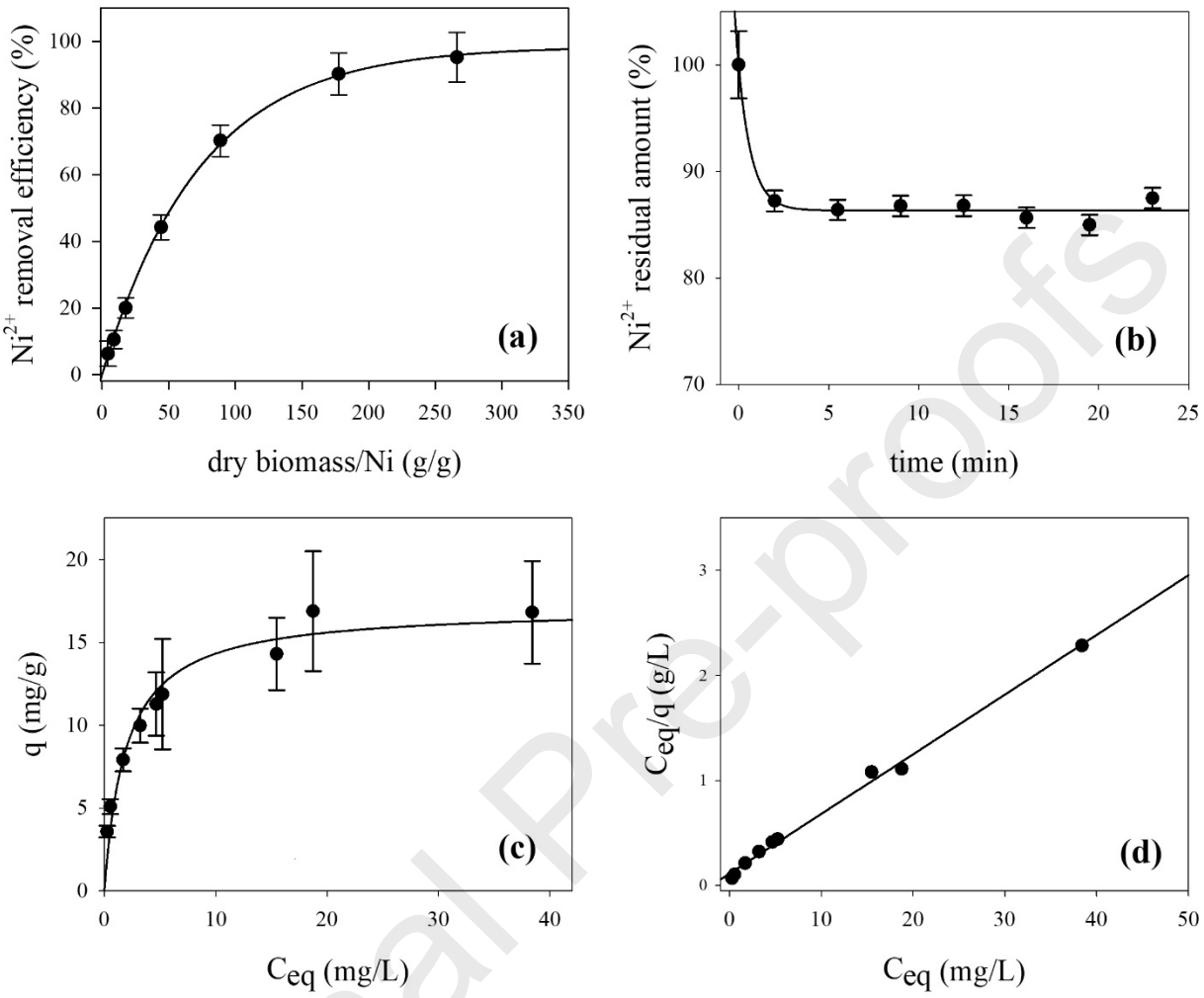

Figure 1. (a) Ni^{2+} removal efficiency as a function of the ratio between the biosorbent dry mass and the initial metal mass. (b) Representative kinetic profile of Ni^{2+} removal from the aqueous solution at pH 7 using a biosorbent/sorbate mass ratio equal to 9 g/g. (c) Ni^{2+} uptake by *R. sphaeroides* biomass (q) as a function of Ni^{2+} equilibrium concentration (C_{eq}). The solid line represents the Langmuir isotherm curve (see eq. 2) fitted to the experimental sorption data. (d) Linear plot arising from rearrangement of Langmuir isotherm function according to eq. 3

.

Biosorbent	Dehydration T† (°C)	q_{max} (mg/g)	K_L (L/mg)	K_D (μM)	R^2	Ref.
Rhodobacter sphaeroides R26.1	37	17.6±0.5*	0.50±0.10*	34±7*	0.995*	this work
***Bacillus cereus* M^1_{16}**	70	344.8#	0.987#	17#	0.987#	[46]
***Lysinibacillus* BA2**	70	180.5 # 129.7*	88.1# 90.5*	0.20# 0.19*	0.951# 0.977*	[59]
***Exiguobacterium sp.* ZM-2**	80	20.1# 20.5*	0.426# 0.553*	40# 31*	0.984# 0.991*	[29]
***Acinetobacter baumannii* UCR-2971**	56	8.8#	0.68#	25#	n.a	[60]
Pseudomonas aeruginosa	56	5.7#	1.28#	13#	n.a	[60]
Bacillus thurigiensis	60	35.46#	0.016#	1064#	0.99#	[61]
Arthrobacter sp.	80	12.7*	0.14*	122*	n.a.	[62]

*live non-growing cells
#dead dried cells
†only for dry weight determination in the case of live cells

Table 1. Dehydration temperature and Langmuir parameters obtained from fitting of Ni^{2+} sorption isotherms relevant to *R. sphaeroides* R26.1 and to other bacterial strains described in the literature.

The Langmuir equation can be rearranged to contain K_D, which is the reciprocal of the Langmuir constant:

$$q = \frac{q_{max} C_{eq}}{K_D + C_{eq}} \qquad (eq.4).$$

The equation above, which describes ligand binding processes by a one-site saturation model, clearly highlights the meaning of K_D, which indeed represents the sorbate equilibrium concentration at which half of the available binding sites are occupied ($q = q_{max}/2$). Hence this

parameter gives immediate information on the affinity of the sorbate for the sorbent phase. Specifically, low values of K_D indicate that available binding sites are easily loaded and are consistent with superior biosorption performances even in presence of q_{max} values not particularly high. The value of 34 μM (0.6 μg/L) found for *R. sphaeroides* indicates that half-saturation of the biosorbent is reached at an equilibrium concentration sufficiently low and suitable for decontamination purposes, considering that the European Union, with its Directive (EU) 2020/2184 of 16 December 2020 on the quality of water intended for human consumption, recommends for drinking water nickel levels below 20 μg per liter[63].

The comparison with data relevant to analogous bacterial adsorbents described in the literature (Table 1) revealed that a strong variability exists regarding to both loading capacity (q_{max}) and sorbate affinity (K_D). The *R. sphaeroides* biomass sorption parameters, extrapolated from metal uptake measurements, proved to be very close to those of *Exiguobacterium sp*[29]. The maximum uptake capacity of *R. sphaeroides* exceeds that of *Acinetobacter baumannii*[60], *Pseudomonas aeruginosa*[60] and *Arthrobacter sp*[62], but is lower than that of *Bacillus cereus*[46] and *Lysinibacillus*[46]. On the other side, the Langmuir constant and the relevant half-saturation concentration are in line with most bacterial adsorbents listed in Table 1, except for *Lysinibacillus*[59] and *Bacillus thurigiensis*[61], which show significantly higher and lower Ni^{2+} affinity respectively. It should be mentioned that specific values of Langmuir parameters can be meaningfully affected by the experimental conditions employed, such as biomass dehydration temperature, which can influence the determination of adsorbent dry weight and consequently the resulting q values. As reported in Table 1, most authors performed dehydration at temperatures over 50°C, while in our case a lower temperature (37°C) was adopted, leading likely to higher dry weights and lower q values.

R. sphaeroides biomass seemed however to adhere particularly well to the requirements of an ideal sorbent surface according to the Langmuir model, as indicated by the R^2 value, the highest in Table 1. This finding suggests that, despite the chemical complexity of the bacterial surface, one specific functional group is mainly involved in nickel binding, a result again in agreement with our previous FTIR study[23], which assigned to carboxylate groups a major role in metal cation uptake. It is interesting to outline that our Ni^{2+} uptake experiments have been carried out with intact cells, which can be considered "non-growing" while interacting with the metal, given the short incubation time and the absence of nutrients in the metal solution. The lack of biomass dehydration likely contributes to preserve the cell surface integrity, favoring its ideal behavior as sorbent surface. With a R^2 value equal to 0.991, live non-growing cells of *Exiguobacterium* proved indeed to adhere equally well to the Langmuir adsorption model[29], while dried cells of the same strain resulted in a lower value. An analogous behavior was observed for *Lysinibacillus* cells[59].

3.2 Elemental composition of dry cell surfaces by XPS

XPS analysis allowed assessing the effect of Ni^{2+} exposure on the chemical composition of *R. sphaeroides* cell surface. A first evaluation of chemical composition changes occurring under Ni^{2+} stress was conducted by comparing the survey spectra of the dry films of control and Ni^{2+}-exposed cell samples (Figure S1). Specifically, intense characteristic carbon (C1s) and oxygen (O1s) peaks are well evident in all XPS profiles with the associated Auger signals C(KLL) at 1223.2 eV BE[64] and O(KLL) at 976.1 eV BE. Nitrogen (N1s), sulphur (S2p, S2s) and phosphorus (P2p, P2s) peak signals are also well marked in all assayed samples. Moreover, other expected elements (i.e. K, Ca, Mg and Ni) were detected. As mentioned above, the total absence in the survey spectra of all analyzed samples of silicon peaks (Si2p and Si2s), arising from the glass surface of the material

used as support, confirmed the uniformity of the cellular layer, whose compactness was sufficient to avoid silicon signal interference in sample spectra.

The detailed HR regions of all peaks of interest were also acquired to achieve the elemental composition of bacterial cells differently treated. The hystograms of relevant atomic distributions are shown in Figure S2. Chemical speciation for any element was obtained after an accurate curve fitting procedure and relevant BE and atomic percentages (At%) are reported in Table 2. Fit parameters for all spectra are listed in Table S2.

Interestingly, a detectable potassium peak signal (K2p), related to K^+ ions, was observed only in the control sample (1.9±0.1%), while the nickel signal (Ni2p), totally absent in the control, was observed in both samples exposed to nickel chloride (1.1± 0.1% for Ni1.2 and 1.2±0.1% for Ni12 samples respectively). Moreover, the total absence of any chlorine species in $NiCl_2$-treated cells allowed excluding that nickel came from nickel chloride contamination. All these results highlight the ability of phototrophic cells to capture nickel species, lowering drastically the amount of interacting K^+ ions that in our treated samples were almost totally replaced by Ni^{2+}. This phenomenon is well evident looking at the typical HR XPS spectra of C1s-K2p and Ni2p regions (Figure 2): only trace amount of potassium (lower than 0.08%) were present in cells exposed to both tested $NiCl_2$ concentrations since K^+ signals were barely detectable.

Although divalent cationic species, i.e. Ca^{2+} and Mg^{2+}, proved to be present on both control and $NiCl_2$ treated cells, Na^+ cations were absent in all samples. This finding demonstrates that, according to Borrok et al.[50], the washing step with KCl 0.1 M at neutral pH results in a preferential displacement of monovalent cations (i.e. Na^+) by K^+ ions, which in turn are efficiently exchanged with Ni^{2+} ions in case of Ni^{2+} exposure.

Element	comp.	Assigned speciation	Ctrl cells			Ni 1.2 cells			Ni 12 cells		
			BE (eV)	At%		BE (eV)	At%		BE (eV)	At%	
C1s	**C1**	**C**-(H,R) **C**=C	285.0	30.2±0.3	62.7±0.1	285.0	32.1±0.7	64.2±0.1	285.0	33±3	64.2±0.2
	C2	O=C-**C**$_{\alpha}$	286.0	6.9±2.6		286.1	6.7±2		286.1	7±3	
	C3	-**C**-(O,N)	286.6	15.6±3.0		286.7	15.4±1		286.7	15±4	
	C4	O=**C**-(C,N) O=**C**-O$^-$ O-**C**-O	288.0	7.6±0.2		288.1	7.4±0.1		288.1	7±2	
	C5	O=**C**-O-H O=**C**-O-C	289.1	2.5±0.2		289.1	2.5±0.2		289.1	2.5±0.5	
N1s	**N1**	-C=**N**-C	398.6	0.18±0.03	4.8±0.2	398.1	0.14±0.01	5.6±0.3	398.0	0.16±0.03	6±1
	N2	O=C-**N** -C-**N**	400.1	4.0±0.3		400.2	4.6±0.1		400.2	4.8±2	
	N3	C-**N**H$_3^+$	401.6	0.31±0.01		401.6	0.5±0.2		401.3	0.50±0.01	
	N4	R$_4$-**N**$^+$	402.8	0.3±0.1		402.8	0.4±0.1		402.5	0.4±0.2	
O1s	**O1**	**O**=C- **O**=C-**O**$^-$	531.6	8.9±0.4	28.4±0.3	531.9	9.7±0.1	27.3±0.5	531.8	10.4±0.5	27.2±1
	O2	-C-**O** O=C-**O**-C O=C-**O**H	532.9	18.6±0.9		532.9	15±1		532.9	14±1	
	O3	H-**O**H	534.3	0.8±0.3		534.0	2.5±0.5		533.7	2.8±0.8	
S2p$_{3/2}$	**S1**	C-**S**-	163.9	0.03±0.05	1.32±0.06	163.9	0.07±0.01	1.20±0.06	164.0	0.03±0.04	1.13±0.03
	S2	C-**S**O$_3^-$	168.6	1.29±0.01		168.8	1.13±0.05		168.7	1.0±0.2	
P2p$_{3/2}$	-C-O-**P**O$_3^{2-}$		133.4	0.67±0.02		133.8	0.42±0.01		133.7	0.37±0.04	
Ca2p$_{3/2}$	**Ca^{2+}**		347.4	0.04±0.05		347.8	0.02±0.02		347.8	0.01±0.02	
K2p$_{3/2}$	**K$^+$**		293.2	1.85±0.04		293.1	0.07±0.01		293.2	traces	
Mg2s	**Mg^{2+}**		89.1	0.20±0.03		89.5	0.14±0.01		89.3	0.16±0.15	
Ni2p$_{3/2}$	**Ni^{2+}**		------	------		856.5	1.1±0.1		856.5	1.2±0.1	

Table 2. Atomic percentage surface concentration (At%) and relevant BEs of the elements in different chemical states as arising from fitting of the HR regions with individual element peaks. Peak assignments refer to literature data and to the NIST standard reference database available on line[55].

Moreover, these results suggest that the experimental conditions for sample dehydration and XPS analysis do not compromise dramatically the integrity of cells, and any release of cytosol material (i.e. Na^+ and Cl^-), reaching the outermost layer of the sample, can be excluded.

As arises from At% data in Table 2, the ratio between Ni^{2+} in $NiCl_2$-treated samples and K^+ in control cells is around 1:2, which is the expected value assuming a quantitative K^+/Ni^{2+} cation exchange. While a substantially complete displacement of potassium ions occurred for both $NiCl_2$ tested concentrations, only a minor Ni^{2+}-induced decrease of Ca^{2+} and Mg^{2+} divalent ion signals was observed.

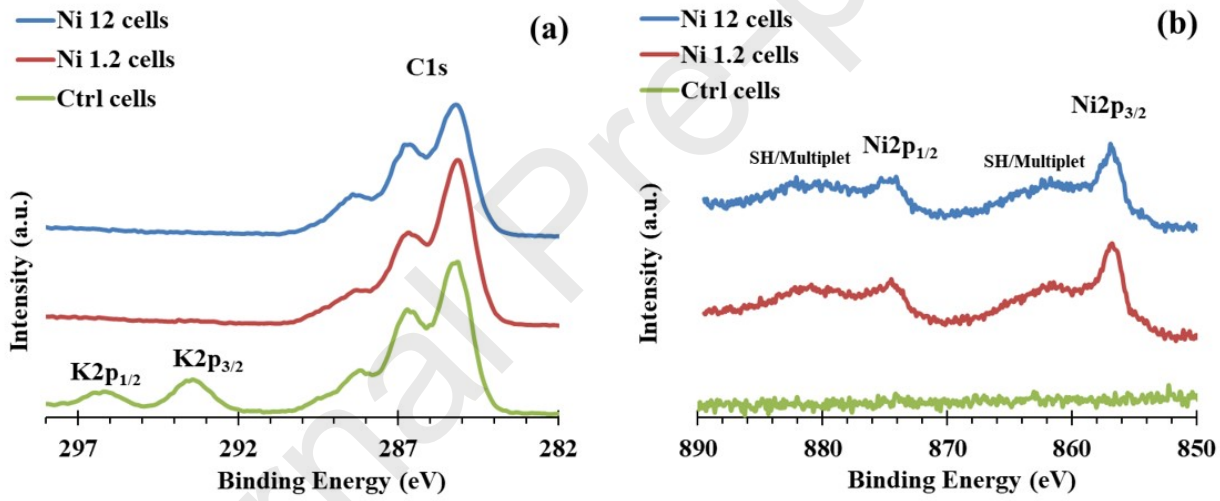

Figure 2. HR XPS spectra of Ctrl, Ni1.2 and Ni12 cell samples showing C1s-K2p (a) and Ni2p (b) regions.

It is well known that the cell envelope of most bacteria is negatively charged [65] due to the presence of carboxylate and phosphate groups [66], which account for the cation adsorption ability of microbial biomass. Sulphated saccharides [67] may also contribute to the negative charge of the bacterial surface. The maximum cation uptake capacity arising from electrostatic interactions is determined by the extent of the negative charge on the bacterial surface and therefore by the amount of these anionic functional groups. It should be mentioned that in the case of transition

metal cations, such as nickel(II), the establishment of covalent coordinative bonds, even with uncharged groups, is also feasible widening the number and typology of binding events. On the basis of the fairly quantitative potassium cation exchange observed, the Ni^{2+} binding to uncharged groups seems to be minor. Nevertheless, unlike potassium ions, which is a hard ion involved in outer sphere interactions[24], the chemical characteristics of nickel ion suggest inner-sphere interactions with anionic groups, which imply a more pronounced chemical modification of the surface, as usually occurs for chemisorption processes.

The relative content of macroelements of the cell envelope (C, O and N) as well as S and P, was found quite similar for all analyzed samples. However, the atomic ratios of elements, in terms of O/C, N/C, P/C and S/C values, widely used to assess and compare the chemical composition of bacterial cells by XPS[42], pointed out slight but significant variations ascribable to $NiCl_2$ treatment. Specifically, Ctrl cells showed O/C, N/C, P/C and S/C surface concentration ratios equal to 0.453, 0.077, 0.0107 and 0.021, respectively. After $NiCl_2$ treatment, only the N/C and P/C ratios changed. Both Ni1.2 and Ni12 cell samples were higher in nitrogen content (average N/C=0.09) and lower in phosphate (average P/C=0.0062), while oxygen (average O/C=0.42) and sulphur (average S/C=0.018) were substantially constant. All data and relevant errors are reported in Table S2. These results indicate that the presence of nickel in substitution of potassium promotes a different distribution of phosphate and amine /amide groups in the probed sample thickness, with an N/P surface concentration ratio almost two-fold higher than the N/P measured on the Ctrl cells. As a matter of fact, our XPS results indicate that no significant differences exist between surface chemical composition of bacterial cells exposed to 1.2 mM and 12 mM Ni^{2+} concentration, demonstrating that a substantial saturation of binding sites occurs at concentration >1.2 mM, in

nice agreement with the K_D parameter (34 μM) arising from adsorption isotherm. The samples Ni1.2 and Ni12 can be therefore considered as replicates of a Ni^{2+} fully saturated bacterial surface.

3.3 Cell surface functional groups probed by XPS

The assessment of specific speciation of any element and relevant estimation of functional group distribution provided information complementary to the elemental analysis, enabling a deeper characterization of bacterial surfaces both nickel-free and after nickel biosorption. Accurate curve-fitting procedures of HR XPS spectra of macroelements allowed to accomplish this task. Since, as discussed above, the profiles obtained for HR spectra of Ni12 sample proved to be very similar to those relevant to Ni1.2 sample, only the latter were reported in Figure 3 and compared with Ctrl spectra. However, all XPS data, arising from fitting of Ctrl, Ni1.2 and Ni12 HR spectra are listed in Table 2.

Panels (a) and (b) of Figure 3 show best fitting curves to the HR scan of C1s region for Ctrl and Ni1.2 cell samples. The broad and asymmetric features of C1s signals clearly suggested the multiple peak contribution to HR profile, highlighting the presence of chemically different carbons. To quantify the components of C1s signal, the carbon was classified into five different typologies: i) aliphatic carbon (285.0 eV), ii) alpha carbon to a carboxylic/amide group (286.0 eV)[68–70], iii) alcoholic and amino carbon (286.6 eV), iv) carbonyl, amide and hemiacetal/acetal carbon (288.1 eV), and v) protonated carboxylic and ester carbon (289.1 eV)[71]. C1s BE attributions and relative At% are quite similar for all assayed biosurfaces and consistent with the typical chemical composition of bacterial cell envelopes, whose main components are lipids, proteins and carbohydrates, each one characterized by specific and well identified functional groups[71].

Likewise, the related N1s peak signals, shown in panels (c) and (d) of Figure 3, were successfully fitted with three main nitrogen components usually present in biological samples: i) amide/unprotonated amino nitrogen (400.2-400.1 eV), ii) protonated amino nitrogen (401.6-401.3 eV)[70], and iii) quaternary ammonium (402.8-402.5)[71]. Only traces of a fourth component, labelled as N1 in the relevant graphs and in Table 2, were detected and assigned to imide nitrogen, mainly arising from histidine and arginine residues of proteins [70]. In agreement with the biological nature of our samples and the typical composition of a Gram-negative envelope, nitrogen is present in the organic matrix primarily as amino/amide groups, likely originating from proteins associated to the outer membrane and from peptidoglycan[70]. The quaternary ammonium could be attributed to phosphatidylcholine (PC) lipids, bearing a N,N,N-trimethyl ethanolammonium cation in the head group. It was indeed demonstrated that *R. sphaeroides* is able to synthetize this phospholipid thanks to a phospatidylethanolamine (PE) methyltransferase, which is homologous to the one of *Pseudomonas aerouginosa*[72]. Moreover, in the latter strain PC was demonstrated to be located within the outer membrane (inner leaflet) as well as in the cytoplasmic membrane[73]. On the other side, the protonated amino nitrogen signal can be attributed to basic amino acid residues and to PE, which is one of the main lipid constituent of the inner leaflet of the outer membrane of Gram-negative bacteria[74]. In general, the quantitative analysis showed a nitrogen surface enrichment in the case of Ni^{2+}-treated samples, supporting the hypothesis that nickel ions play a role in making nitrogen-rich components more exposed to the exterior and therefore more accessible to the probing radiation.

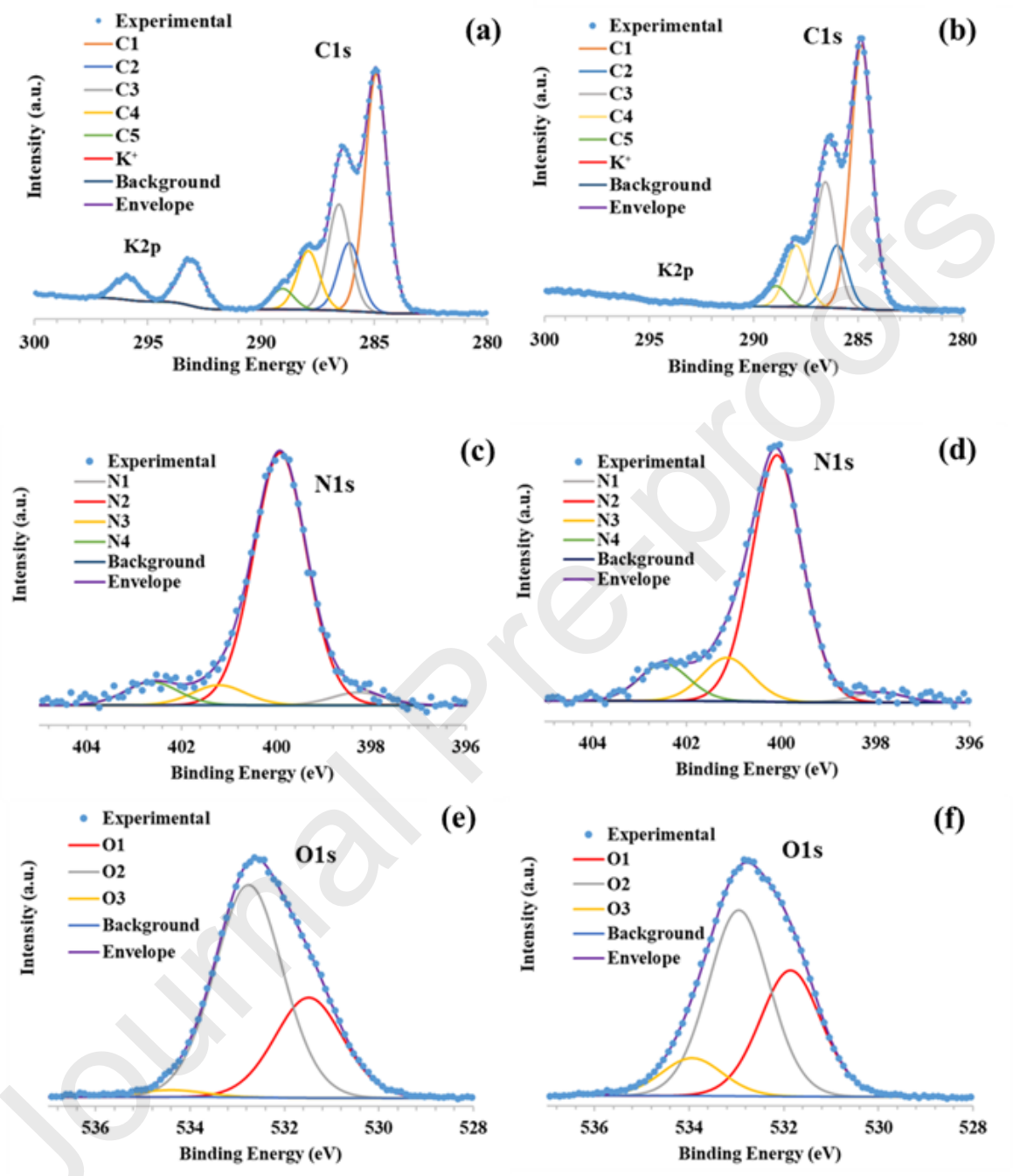

Figure 3. Typical HR XPS spectra of C1s/ K2p (a,b), N1s (c,d) and O1s (e,f) regions and relevant curve fitting for Ctrl (a,c,e) and Ni1.2 (b,d,f) cell samples. Refer to labels in Table 2 for the functional groups assigned to the individual signal components indicated in the legends.

Peak signals attributed to O1s from Ctrl cells (Figure 3e) were fitted with two principal components that originate from i) doubly bound oxygen in carbonyl, amide and carboxylate groups at 531.6 eV and ii) singly bound oxygen in alcoholic, carboxyl and ester groups at 532.9 eV[69]. The average ratio C-O/C=O obtained from the fitting is around 2:1. A third and very weak component at higher BE (534.1eV), with an atomic percentage around 0.8, was attributed to -O-H groups of residual water present in cell samples[75]. The typical O1s peak for Ni1.2 sample is reported in panel (f) of Figure 3. Again, the asymmetric peak shape can be fitted by using three components. The most intense component at 532.9 eV as well as the component at 531.8 eV were attributed to the same oxygen species found in Ctrl samples. However, the new average ratio C-O/C=O in Ni^{2+}-treated samples proved to be lower, around 1.45: 1. This remarkable change can be referred to the increase of the peptide content with respect to the saccharide component, causing the relative reduction of alcohol and (hemi)acetal C-O signal, in agreement with the trend of nitrogen signals, showing an increase of amide contribution.

These results can be examined on the basis of the information depth of XPS (around 10 nm) and the thickness of cell envelope components in Gram-negative bacteria. Ultrastructure analysis of the cell envelope of *R. sphaeroides* reported a 17.9 nm thick periplasmic space[76], suggesting that only the outer membrane and part of the periplasmic peptidoglycan layer are probed during XPS analysis. This assumption is in agreement with the observations of Ramstedt and coworkers[77], who attributed their XPS signals to the outer-most part of the cell envelope.

As a matter of fact the dehydration step and the ultra-low pressure conditions under analysis might affect strongly the intergrity and the structural arrangement of the different components. However, despite the simplicity of our dehydration procedure, cell rupture and release of cytosol material can be excluded given the absence of any Na^+ and Cl^- signals in XPS spectra. We outline that

rinsing the sample with distilled water, as in our case, was found to protect cells from cell damage during drying[78]. Even though a dehydration-induced rupture of the sole outer-most layer of the cell envelope resulting in the exposure of cytoplasmic membrane cannot be ruled out, our spectra of untreated cells seem more consistent with the contribution to the observed XPS signals of only outer membrane and perhaps a portion of peptidoglycan. Specifically, it is likely that Ctr cells spectra contain a more pronounced contribution by the outer leaflet of outer membrane, with stronger saccharide signals arising from the lipopolysaccharide (LPS) component, while the Ni^{2+}-treated cells present bigger contributions from the inner leaflet of outer membrane (quaternary ammonium and protonated amine arising from PC and PE head groups of lipids respectively) and from the peptidoglycan layer (increased amide nitrogen). In addition, the slight enhancement of aliphatic carbon and quaternary ammonium signals in Ni^{2+}-treated samples may also suggest that cytoplasmic membrane, with fatty acids and choline haedgroups, contributes partly to relevant XPS profiles. On the basis of these findings we suppose that K^+ replacement with Ni^{2+} in cell envelope strongly affects the structural arrangement of the different chemical components on the cell envelope.

It is well-known that divalent cations, such as Ca^{2+} and Mg^{2+}, favor tight packing and stability of LPS layer within a model membrane[79,80]. Moreover, it has recently been shown that, in a native state outer membrane, LPS is organized in patches[81] greatly influencing permeability properties. As already highlighted, calcium and magnesium are only slightly diminished in presence of nickel, indicating that the main action of the heavy metal ion is not at the level of phosphate groups interacting with Mg^{2+} and Ca^{2+}, but rather involves anionic groups physiologically interacting with alkali monovalent cations. Interestingly, the slight decrease of Mg^{2+} and Ca^{2+} is accompanied by a simultaneous reduction of phosphate groups (see Table 2), implying that a unique chemical

component is actually diminished in the case of Ni^{2+} treatment. This finding further supports the hypotesis that outer membrane LPS, with its phosphate moieties stabilized by Mg^{2+} and Ca^{2+} is relatively less abundant across the information depth and contributes to a lesser extent to the overall XPS spectrum of samples exposed to Ni^{2+}.

Comparing Ni^{2+} and K^{+}, in terms of ionic radius (0.72Å[82] and 1.33Å[83] respectively) and electronic properties, it is expected that the smaller size of nickel(II) joined to feasible inner-sphere interactions with carboxylate groups favors stacking of carboxylate-rich saccharide chains at the level of outer membrane LPS. Interestingly, a recent study on model membranes reported that Ni^{2+} ion binding to the charged groups of the O-antigen units of LPS from *Salmonella Enterica* would preserve the lipid bilayer structure, while the absence of the outermost saccharide moiety would induce the complexation of groups at the level of the inner-core saccharide, causing a deformation of the lipid bilayer[84]. The specific characteristics of *R. sphaeroides* LPS may affect strongly the response of outer membrane organization and morphology to the nickel binding. However, our XPS data demonstrated that considerable changes occur, causing a redistribution of chemical components (peptides, saccharides, lipids) probed by the X-ray beam. In general, in presence of nickel a more pronounced relative contribution of inner layers, i.e. peptidoglycan and cytoplasmic membrane, was observed, which could be in line with increased stacking of LPS saccharide chains (see Figure 4) likely producing wider holes in the characteristic net-like structure recently reported[81]. In this case porins and inner layers would be more exposed to the surface, contributing more significantly to the XPS spectrum. Of course, the transition from the wet state to the dry state might result in a more disordered arrangement due to the collapse of the envelope components to the surface. Nevertheless, our data suggest that, even in presence of further modifications induced by cell water loss, the resulting dry biosurfaces still show clear differences

between control and Ni^{2+}-exposed cells, pointing out the strong ability of this ion to affect envelope organization.

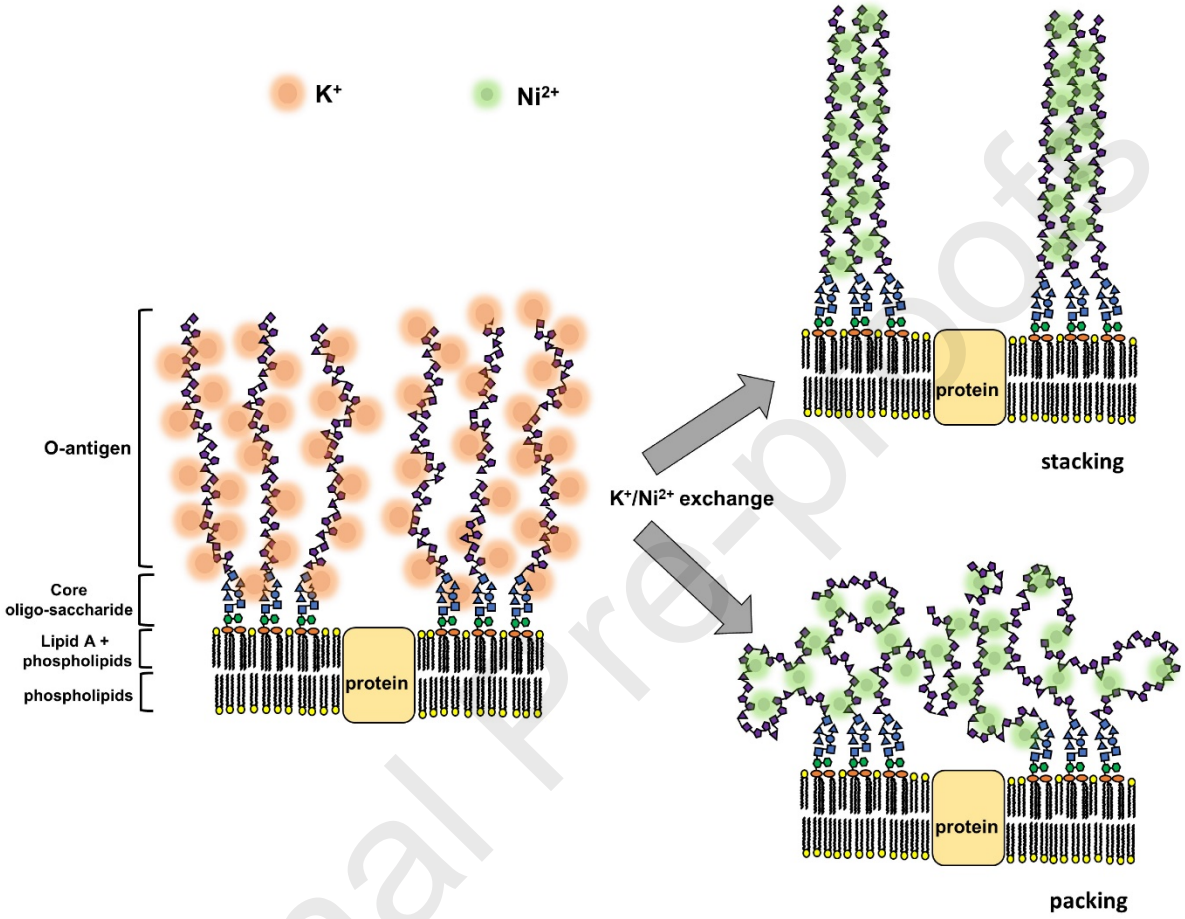

Figure 4. Schematic representation of two possible scenarios following K^+/Ni^{2+} exchange on the cell surface of *R. sphaeroides*, both in line with XPS observations. Smaller size, coordinative properties and cross-linking action of Ni^{2+} ions are expected to induce either lateral (stacking) or horizontal (packing) compression of LPS sugar chains.

The O1s signal region shows in addition a third component at high BE (534.3 eV) that proved to be downshifted and more abundant in the case of nickel treated samples. We tentatively assign this component to OH from ligand water since its enrichment in the case of Ni1.2 and Ni12 samples

might be neatly explained with the presence of metal-coordinated water at the level of Ni^{2+} complexes. The coordination number of this divalent cation can indeed vary from four to six.

Sulphur spectra observed in all analyzed samples showed S2p signals characterized by two components: a dominant well resolved asymmetric peak and a small one at lower BE, according to the presence of two different sulphur chemical species. The representative S2p HR spectrum of Ctrl cells is shown in panel (a) of Figure S3. Ni-treated cells spectra are not shown since they are very similar to Ctrl ones. The S2p peak signal at higher BE consists of a spin-split doublet $S2p_{1/2}$ and $S2p_{3/2}$, with energy splitting of 1.2 eV and relative intensity ratio about 1:2, in agreement with previously reported studies[85–87]. The second peak was instead fitted with a single component as it was too weak to be resolved. Based on the $S2p_{3/2}$ BE, the most intense peak can be attributed to sulphate/sulphonate species (168.8-168.6 eV) while the less intense one can be ascribed to organic sulphides (C-S-), present as traces[85], in agreement with XPS features (BE=163.6-164 eV) reported for cysteine incorporating peptides[55,70].

The observed sulphate/sulphonates can be associated to sulphated saccharides from the outer membrane, which have been observed not only in cyanobacteria[88] but also in proteobacteria[89] and to anionic sulpho-glycerolipids, whose presence in *R. sphaeroides* cell membrane has been demonstrated[90]. Particularly abundant was indeed found the characteristic non-phosphorous glycolipid sulpho-quinovosyldiacylglycerol, a peculiar component of purple bacteria photosynthetic membrane[91]. In general, sulphate/sulphonate signals proved to be rather intense, with At% higher than those of phosphates, pointing out the high content of sulphated saccharides and/or lipids occurring in this strain. Table 2 shows that only a slight relative reduction of sulphur was observed in the case of Ni^{2+}-treated samples.

The P2p peak signals were found likewise qualitatively similar in control and nickel treated cells and are consistent with a single phosphate component at 133.4-133.8 eV BE attributed to organic phosphate ions[92], coming from LPS and phosphoglycerolipids[91]. The representative P2p HR spectrum of Ctrl cells is shown in panel (b) of Figure S3. Despite the qualitative similarity, the overall reduction of phosphate signal intensity in the case of Ni^{2+}-treated samples (see data in Table 2) may be ascribed to the higher relative contribution to the XPS spectra of unphosphorylated moieties, such as proteins and peptidoglycan. Crossing At% concentrations of phosphate (decreasing in the case of nickel exposure) and quaternary ammonium (increasing in the case of nickel exposure), it is possible to conclude that the overall phosphate decrease is accompanied by a higher relative content of PC lipids, further supporting the hypothesis that the membrane components are differently exposed to the surface. Specifically, PC is located in the inner leaflet of the outer membrane and in the cytoplasmic membrane, thus suggesting that either wider holes are present in the outermost layer, or the thickness of the outermost layer is reduced. Stacking (lateral compression) or packing (horizontal compression) of LPS saccharides (see Figure 4) would be both in line with these observations.

3.4 Metal speciation by XPS

Ca2p, Mg2s and K2p peak signals of calcium, magnesium and potassium microelements were easily assigned to Ca^{2+} ($Ca2p_{3/2}$, BE=347.4-347.8 eV), Mg^{2+} (Mg2s, BE=89.1-89.5 eV) and K^{+} ($K2p_{3/2}$, BE=293.3 eV) ions [55].

To confirm that the bacterial surface immobilizes nickel as divalent cations, the Ni2p HR spectra of Ni1.2 and Ni12 cell samples were compared with HR spectrum of $NiCl_2$, used as standard for nickel(II) species. As shown in panel (b) of Figure 5, the Ni2p signal of $NiCl_2$ is composed of an intense peak at 856.4 eV ($Ni2p_{3/2}$) and a second one (not shown in the figure) at 873.8 eV ($Ni2p_{1/2}$),

associated to the characteristic satellites that represent the fingerprint for the recognition of high-spin nickel(II), a behavior consistent with a $3d^8$ nickel(II) ion[93,94]. The modified Auger parameter was found equal to 1698.92±0.20 eV, which is in line with the value reported in the literature (1698.65 eV)[93]. An intense Cl2p peak signal was also detected (spectrum not shown). Likewise, the Ni2p peak shape detected in cell samples exposed to the metal (Figure 5a) presented an intense peak pair at 856.5 eV ($Ni2p_{3/2}$) and at 873.5 eV ($Ni2p_{1/2}$), associated as well to satellites distinctive of a $3d^8$ high-spin nickel(II) ion. Nevertheless, the empirical curve fitting conducted with the same optimized fit parameters used for deconvolution of $NiCl_2$ $Ni2p_{3/2}$ signal, highlighted some differences. Specifically, $Ni2p_{3/2}$ peak of cell samples could be deconvoluted by using 4 peak components, with FWHMs higher than those observed in $Ni2p_{3/2}$ signal relevant to $NiCl_2$. Both the modified Auger parameters for Ni1.2 and Ni12 cells samples were found equal to 1698.6±0.2 eV (see Table S1), in nice agreement with the values reported for $NiCl_2$ [93] and organic Ni^{2+} complexes (i.e. nickel-acetylacetonate)[95]. This findings allowed to safely assign nickel signals to nickel divalent cation species.

Clearly, the separation of multiplet and shake-up (SH) satellites in the $Ni2p_{3/2}$ region was too low in these samples to be deconvoluted with the same details as in $NiCl_2$ standard, where 8 peak components could be easily resolved. In addition, near the $Ni2p_{3/2}$ most intense component it was here evident the presence of traces of a chemically different nickel(II) species as inferred from the weak but well resolved $Ni2p_{3/2}$ peak signal at 854.21 eV coupled with $Ni2p_{1/2}$ at 873.64 eV[93]. The specific $Ni2p_{3/2}$ BE (856.5 eV), combined with a different Ni2p signal shape and the absence of Cl^- counter ions, agrees with the occurrence of specific nickel ion chemical interactions with negative functional groups lying on the bacterial cell, mostly carboxylates, following displacement of electrostatically bound potassium cations [96].

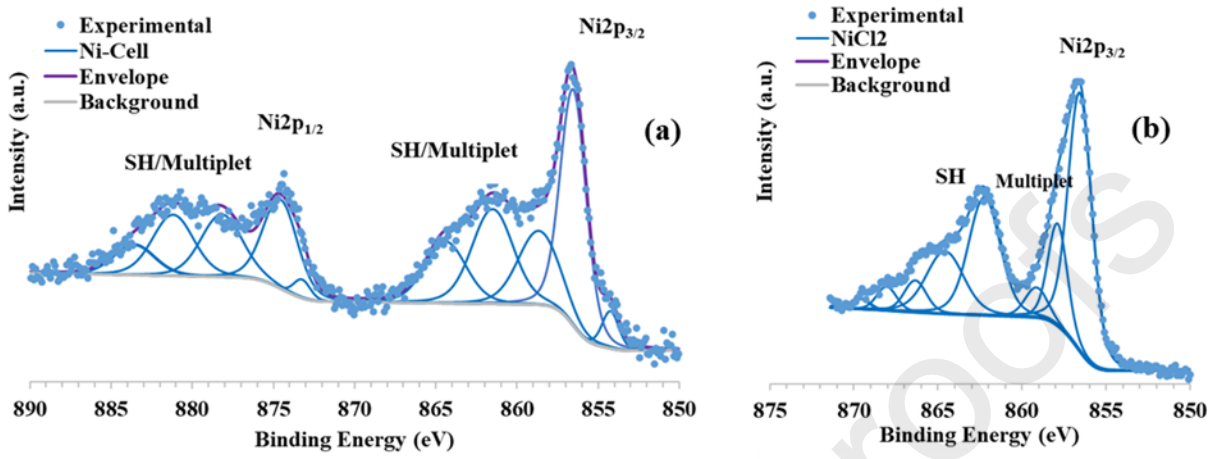

Figure 5. Ni2p regions of XPS HR spectra and relevant curve fitting for Ni1.2 cells (a) and for the standard compound $NiCl_2$ (b)

4. CONCLUSIONS

Nickel(II) uptake measurements, conducted with intact non-growing cells of *R. sphaeroides,* demonstrated that the cell envelope of this Gram-negative bacterium behaves as an ideal adsorbent surface, showing non interacting and chemically equivalent binding sites, which get half-saturated at an equilibrium concentration of 34 µM and can load up to 17.6 mg of nickel per gram of dried biomass.

The XPS analysis of nickel-saturated dry biomass outlined a quantitative displacement of K^+ ions by Ni^{2+}. The absence of any XPS signal arising from cytosol marker constituents, such as sodium and chloride, demonstrated that the biomass, suitably washed with distilled water and dried at ambient temperature and pressure, does not undergo cell lysis during analysis under high vacuum.

Curve fitting of HR signals allowed assessing that a clear modification of the cell surface is induced by Ni^{2+} binding in terms of distribution of main chemical components. Specifically, peptide and choline lipid content proved to increase, while functional groups associated to saccharide components decreased. The relative content of Ca^{2+} and Mg^{2+} decreased only slightly as well as phosphates, suggesting that these divalent cations remain tightly bound to phosphate groups of lipid A and inner-core saccharide, thus ensuring LPS stability. Functional group distribution and charge balance allowed assessing that Ni^{2+} does not interact with phosphates, being instead mostly coordinated by carboxylate groups, with only a minor role played by the interaction with sulphonates. Although investigations with further techniques are needed for assessing actual morphological and structural changes occurring at the level of the outer membrane, our data strongly suggest chemical arrangement modifications induced by Ni^{2+} inner-sphere interactions with carboxylate moieties, resulting likely in stacking and/or packing of saccharide chains of LPS. The major involvement of carboxylate functional groups in nickel extracellular uptake by *R. sphaeroides* agrees with previous FTIR data[23] and with the successful modelling by the Langmuir equation.

These results further outlined the potential of XPS technique for the quantitative assessment of cation exchange processes occurring at the surface of a complex biosystem, such as the microbial cell, delivering valuable information not only on the functional groups involved in the binding, but also on the influence of metal ions on the supramolecular organization of the bacterial envelope. In this context XPS technique proved to be a powerful technique for investigating possible heavy metal stress/toxicity mechanisms involving the surface of aquatic (micro)organisms.

AUTHOR INFORMATION

Corresponding Author

*Livia Giotta (livia.giotta@unisalento.it)

Author Contributions

The manuscript was written through contributions of all authors. All authors have given approval to the final version of the manuscript.

ACKNOWLEDGMENTS

The authors are grateful to Gianroberto Zingarofalo and Giorgio Martina for their support in conducting biosorption measurements. This research was financially supported by MUR (Ministero dell'Università e della Ricerca) in the framework of the program PON-AIM (Programma Operativo Nazionale-Attrazione e Mobilità Internazionale dei Ricercatori), Grant AIM1882733.

SUPPLEMENTARY INFORMATION:

Modified Auger parameter (α') determination, XPS peak fitting procedure, Table S1, Table S2, Table S3, Figure S1, Figure S2, Figure S3

REFERENCES

[1] J. Briffa, E. Sinagra, R. Blundell, Heavy metal pollution in the environment and their toxicological effects on humans, (2020). https://doi.org/10.1016/j.heliyon.2020.e04691.

[2] J.P. Vareda, A.J.M. Valente, L. Durães, Assessment of heavy metal pollution from anthropogenic activities and remediation strategies: A review, J. Environ. Manage. 246 (2019) 101–118. https://doi.org/10.1016/j.jenvman.2019.05.126.

[3] W.X. Wang, Interactions of trace metals and different marine food chains, Mar. Ecol. Prog. Ser. 243 (2002) 295–309. https://doi.org/10.3354/meps243295.

[4] M. Jaishankar, T. Tseten, N. Anbalagan, B.B. Mathew, K.N. Beeregowda, A. Blessy, B. Mathew, Toxicity, mechanism and health effects of some heavy metals, (2014). https://doi.org/10.2478/intox-2014-0009.

[5] S. Bettini, R. Pagano, L. Valli, G. Giancane, Spectroscopic Investigation of the Selective Interaction of Mercuric and Cupric Ions with a Porphyrin Active Layer, J. Phys. Chem. C. 118 (2014) 12384–12390. https://doi.org/10.1021/jp503292r.

[6] Cempel M., Nikel G., Nickel: A Review of Its Sources and Environmental Toxicology, Polish J. Environ. Stud. 15 (2006) 375–382. http://www.pjoes.com/Nickel-A-Review-of-Its-Sources-and-Environmental-Toxicology,87881,0,2.html.

[7] S. Buxton, E. Garman, K.E. Heim, T. Lyons-Darden, C.E. Schlekat, M.D. Taylor, A.R. Oller, Concise Review of Nickel Human Health Toxicology and Ecotoxicology, Inorganics. 7 (2019) 1–38. https://doi.org/10.3390/inorganics7070089.

[8] S. Casilli, C. Malitesta, S. Conoci, S. Petralia, S. Sortino, L. Valli, Piezoelectric sensor functionalised by a self-assembled bipyridinium derivative: characterisation and preliminary applications in the detection of heavy metal ions, Biosens. Bioelectron. 20 (2004) 1190–1195. https://doi.org/10.1016/j.bios.2004.04.028.

[9] B. Volesky, Detoxification of metal-bearing effluents: Biosorption for the next century, Hydrometallurgy. 59 (2001) 203–216. https://doi.org/10.1016/S0304-386X(00)00160-2.

[10] A. Hansda, V. Kumar, Anshumali, A comparative review towards potential of microbial cells for heavy metal removal with emphasis on biosorption and bioaccumulation, World J. Microbiol. Biotechnol. 32 (2016) 1–14. https://doi.org/10.1007/s11274-016-2117-1.

[11] M. Zhao, Y. Xu, C. Zhang, H. Rong, G. Zeng, New trends in removing heavy metals from wastewater, Appl. Microbiol. Biotechnol. 100 (2016) 6509–6518. https://doi.org/10.1007/s00253-016-7646-x.

[12] J. Wang, C. Chen, Biosorbents for heavy metals removal and their future, Biotechnol. Adv. 27 (2009) 195–226. https://doi.org/10.1016/j.biotechadv.2008.11.002.

[13] Z. Velkova, G. Kirova, M. Stoytcheva, S. Kostadinova, K. Todorova, V. Gochev, Immobilized microbial biosorbents for heavy metals removal, Life Sci. 18 (2018) 871–881. https://doi.org/10.1002/elsc.201800017.

[14] A. Malik, Metal bioremediation through growing cells, Environ. Int. 30 (2004) 261–278. https://doi.org/10.1016/j.envint.2003.08.001.

[15] S. Rangabhashiyam, E. Suganya, N. Selvaraju, L.A. Varghese, Significance of exploiting non-living biomaterials for the biosorption of wastewater pollutants, World J. Microbiol. Biotechnol. 30 (2014) 1669–1689. https://doi.org/10.1007/s11274-014-1599-y.

[16] Y. Wang, V. Selvamani, I.K. Yoo, T.W. Kim, S.H. Hong, A Novel Strategy for the Microbial Removal of Heavy Metals: Cell-surface Display of Peptides, Biotechnol. Bioprocess Eng. 26 (2021) 1–9. https://doi.org/10.1007/s12257-020-0218-z.

[17] H.A. Alalwan, M.A. Kadhom, A.H. Alminshid, Removal of heavy metals from wastewater

using agricultural byproducts, J. Water Supply Res. Technol. - AQUA. 69 (2020) 99–112. https://doi.org/10.2166/aqua.2020.133.

[18] L. Cutillas-Barreiro, R. Paradelo, A. Igrexas-Soto, A. Núñez-Delgado, M.J. Fernández-Sanjurjo, E. Álvarez-Rodriguez, G. Garrote, J.C. Nóvoa-Muñoz, M. Arias-Estévez, Valorization of biosorbent obtained from a forestry waste: Competitive adsorption, desorption and transport of Cd, Cu, Ni, Pb and Zn, Ecotoxicol. Environ. Saf. 131 (2016) 118–126. https://doi.org/10.1016/j.ecoenv.2016.05.007.

[19] L. Giotta, A. Agostiano, F. Italiano, F. Milano, M. Trotta, Heavy metal ion influence on the photosynthetic growth of Rhodobacter sphaeroides, Chemosphere. 62 (2006) 1490–1499.

[20] A. Buccolieri, F. Italiano, A. Dell'Atti, G. Buccolieri, L. Giotta, A. Agostiano, F. Milano, M. Trotta, Testing the photosynthetic bacterium Rhodobacter sphaeroides as heavy metal removal tool, Ann. Chim. 96 (2006) 195–203.

[21] F. Italiano, A. Buccolieri, L. Giotta, A. Agostiano, L. Valli, F. Milano, M. Trotta, Response of the carotenoidless mutant Rhodobacter sphaeroides growing cells to cobalt and nickel exposure, Int. Biodeterior. Biodegrad. 63 (2009) 948–957. https://doi.org/10.1016/j.ibiod.2009.05.001.

[22] F. Italiano, S. Rinalducci, A. Agostiano, L. Zolla, F. De Leo, L.R. Ceci, M. Trotta, Changes in morphology, cell wall composition and soluble proteome in Rhodobacter sphaeroides cells exposed to chromate, BioMetals. 25 (2012) 939–949. https://doi.org/10.1007/s10534-012-9561-7.

[23] L. Giotta, D. Mastrogiacomo, F. Italiano, F. Milano, A. Agostiano, K. Nagy, L. Valli, M.

Trotta, Reversible binding of metal ions onto bacterial layers revealed by protonation-induced ATR-FTIR difference spectroscopy, Langmuir. 27 (2011) 3762–3773. https://doi.org/10.1021/la104868m.

[24] R.G. Pearson, Hard and Soft Acids and Bases, J. Am. Chem. Soc. 85 (1963) 3533–3539.

[25] I. Langmuir, The adsorption of gases on plane surfaces of glass, mica and platinum, J. Am. Chem. Soc. 40 (1918) 1361–1403. https://doi.org/10.1021/ja02242a004.

[26] J. Febrianto, A.N. Kosasih, J. Sunarso, Y.H. Ju, N. Indraswati, S. Ismadji, Equilibrium and kinetic studies in adsorption of heavy metals using biosorbent: A summary of recent studies, J. Hazard. Mater. 162 (2009) 616–645. https://doi.org/10.1016/j.jhazmat.2008.06.042.

[27] J. Okoli, I. Ezuma, Adsorption Studies of Heavy Metals by Low-Cost Adsorbents, J. Appl. Sci. Environ. Manag. 18 (2014) 443-448–448.

[28] V. Mishra, C. Balomajumder, V.K. Agarwal, Biological removal of heavy metal zinc from industrial effluent by Zinc sequestering bacterium VMSDCM, Clean Technol. Environ. Policy. 16 (2014) 555–568. https://doi.org/10.1007/s10098-013-0655-x.

[29] M.Z. Alam, S. Ahmad, Multi-metal biosorption and bioaccumulation by Exiguobacterium sp. ZM-2, Ann. Microbiol. 63 (2013) 1137–1146. https://doi.org/10.1007/s13213-012-0571-z.

[30] Y. Qu, X. Zhang, J. Xu, W. Zhang, Y. Guo, Removal of hexavalent chromium from wastewater using magnetotactic bacteria, Sep. Purif. Technol. 136 (2014) 10–17. https://doi.org/10.1016/j.seppur.2014.07.054.

[31] A.E. Ofomaja, E.B. Naidoo, Biosorption of lead(II) onto pine cone powder: Studies on biosorption performance and process design to minimize biosorbent mass, Carbohydr. Polym. 82 (2010) 1031–1042. https://doi.org/10.1016/j.carbpol.2010.05.024.

[32] P.B. Dengis, P.A. Gerin, P.G. Rouxhet, X-ray photoelectron spectroscopy analysis of biosurfaces: examination of performances with yeast cells and related model compounds, Colloids Surfaces B Biointerfaces. 4 (1995) 199–211.

[33] H.C. van der Mei, J. de Vries, H.J. Busscher, X-ray photoelectron spectroscopy for the study of microbial cell surfaces, Surf. Sci. Rep. 39 (2000) 1–24. https://doi.org/10.1016/S0167-5729(00)00003-0.

[34] F. Ahimou, C.J.P. Boonaert, Y. Adriaensen, P. Jacques, P. Thonart, M. Paquot, P.G. Rouxhet, XPS analysis of chemical functions at the surface of Bacillus subtilis, J. Colloid Interface Sci. 309 (2007) 49–55. https://doi.org/10.1016/j.jcis.2007.01.055.

[35] P.G. Rouxhet, Y.F. Dufrêne, X-ray photoelectron spectroscopy analysis of the surface composition of Azospirillum brasilense in relation to growth conditions, Colloids and Surfaces. 7 (1996) 271–279. https://doi.org/10.1016/0927-7765(96)01295-7.

[36] L. Leone, J. Loring, S. Sjöberg, P. Persson, A. Shchukarev, Surface characterization of the Gram-positive bacteria Bacillus subtilis-an XPS study, Surf. Interface Anal. 38 (2006) 202–205. https://doi.org/10.1002/sia.2184.

[37] M. Ramstedt, L. Leone, A. Shchukarev, Cell Wall Composition of Bacillus subtilis Changes as a Function of pH and Zn 2+ Exposure: Insights from Cryo-XPS Measurements, Langmuir. 30 (2014) 4367–4374. https://doi.org/10.1021/la5002573.

[38] P. Herben, N. Mozes, P. Rouxhet, Variation of the surface properties of Bacillus licheniformis according to age, temperature and aeration. PG - 184-8, Biochim. Biophys. Acta. 1033 (1990) 184–188. https://doi.org/10.1016/0304-4165(90)90010-t.

[39] H. van der Mei, P. Brokke, J. Dankert, F. Jan, P. Rouxhet, H. Busscher, Physicochemical surface properties of nonencapsulated and encapsulated coagulase-negative staphylococci, Appl. Environ. Microbiol. 55 (1989) 2806–2814. https://doi.org/10.1128/aem.55.11.2806-2814.1989.

[40] K.W. Millsap, G. Reid, H.C. van der Mei, H.J. Busscher, Cluster analysis of genotypically characterized Lactobacillus species based on physicochemical cell surface properties and their relationship with adhesion to hexadecane, Can. J. Microbiol. 43 (1997) 284–291. https://doi.org/10.1139/m97-039.

[41] G. Harkes, H.C. van der Mei, P.G. Rouxhet, J. Dankert, H.J. Busscher, J. Feijen, Physicochemical characterization of Escherichia coli, Cell Biophys. 20 (1992) 17–32. https://doi.org/10.1007/bf02782652.

[42] J.J. Ojeda, M.E. Romero-González, R.T. Bachmann, R.G. J Edyvean, S.A. Banwart, Characterization of the Cell Surface and Cell Wall Chemistry of Drinking Water Bacteria by Combining XPS, FTIR Spectroscopy, Modeling, and Potentiometric Titrations, (2008). https://doi.org/10.1021/la702284b.

[43] Y. Liu, J. Han, S. Dong, Y. Li, S. Liu, Q. Zhou, C. Chen, D.S. Alessi, K.O. Konhauser, H. Zhao, Competitive adsorption of heavy metals by anaerobic ammonium-oxidizing (anammox) consortia, Chemosphere. 258 (2020) 127289.

https://doi.org/10.1016/j.chemosphere.2020.127289.

[44] M. Li, Y. Huang, Y. Yang, H. Wang, L. Hu, H. Zhong, Z. He, Heavy metal ions removed from imitating acid mine drainages with a thermoacidophilic archaea:Acidianus manzaensisYN25, Ecotoxicol. Environ. Saf. 190 (2020) 110084. https://doi.org/10.1016/j.ecoenv.2019.110084.

[45] P. Ding, W. Song, Z. Yang, J. Jian, Influence of Zn(II) stress-induction on component variation and sorption performance of extracellular polymeric substances (EPS) from Bacillus vallismortis, Bioprocess Biosyst. Eng. 41 (2018) 781–791. https://doi.org/10.1007/s00449-018-1911-6.

[46] A. Naskar, A.K. Guha, M. Mukherjee, L. Ray, Adsorption of nickel onto Bacillus cereus M116: A mechanistic approach, Sep. Sci. Technol. 51 (2016) 427–438. https://doi.org/10.1080/01496395.2015.1115069.

[47] K. Zhang, D. Zhang, X. Wu, Y. Xue, Continuous and efficient immobilization of heavy metals by phosphate-mineralized bacterial consortium, J. Hazard. Mater. 416 (2021) 125800. https://doi.org/10.1016/j.jhazmat.2021.125800.

[48] A.L. Neal, K. Lowe, T.L. Daulton, J. Jones-Meehan, B.J. Little, Oxidation state of chromium associated with cell surfaces of Shewanella oneidensis during chromate reduction, Appl. Surf. Sci. 202 (2002) 150–159. https://doi.org/10.1016/S0169-4332(02)00550-0.

[49] H. Zhang, X. Hu, H. Lu, Ni(II) and Cu(II) removal from aqueous solution by a heavy metal-resistance bacterium: kinetic, isotherm and mechanism studies, Water Sci. Technol. 76

(2017) 859–868. https://doi.org/10.2166/wst.2017.275.

[50] D. Borrok, J.B. Fein, M. Tischler, E. O'Loughlin, H. Meyer, M. Liss, K.M. Kemner, The effect of acidic solutions and growth conditions on the adsorptive properties of bacterial surfaces, Chem. Geol. 209 (2004) 107–119. https://doi.org/10.1016/j.chemgeo.2004.04.025.

[51] A.M. Mitchell With M G Mellon, Colorimetric Determination of Nickel with Dimethylglyoxime, Ind. Eng. Chem. Anal. Ed. 17 (1945) 380–382. https://pubs.acs.org/sharingguidelines (accessed July 30, 2021).

[52] D.R. Baer, K. Artyushkova, H. Cohen, C.D. Easton, M. Engelhard, T.R. Gengenbach, G. Greczynski, P. Mack, D.J. Morgan, A. Roberts, XPS guide: Charge neutralization and binding energy referencing for insulating samples, J. Vac. Sci. Technol. A. 38 (2020) 031204. https://doi.org/10.1116/6.0000057.

[53] ISO19318:2021 Surface chemical analysis — X-ray photoelectron spectroscopy — Reporting of methods used for charge control and charge correction Analyse, (2021).

[54] C.D. Wagner, A. Joshi, The auger parameter, its utility and advantages: a review, J. Electron Spectros. Relat. Phenomena. 47 (1988) 283–313. https://doi.org/https://doi.org/10.1016/0368-2048(88)85018-7.

[55] NIST, X-Ray Photoelectron Spectroscopy Database, (n.d.).

[56] D. Briggs, M.P. Seah, eds., Practical Surface Analysis By Auger and X-Ray Photoelectron Spectroscopy., 2nd ed., Wiley, Chichester, 1990.

[57] D. Briggs, J.T. Grant, eds., Surface Analysis by Auger and X-Ray Photoelectron Spectroscopy, IMPublications, Chichester, 2003.

[58] A.M. Salvi, J.E. Castle, The intrinsic asymmetry of photoelectron peaks: dependence on chemical state and role in curve fitting., J. Electron Spectros. Relat. Phenomena. 95 (1998) 45–56. https://doi.org/10.1016/S0368-2048(98)00205-9.

[59] D. Prithviraj, K. Deboleena, N. Neelu, N. Noor, R. Aminur, K. Balasaheb, M. Abul, Biosorption of nickel by Lysinibacillus sp. BA2 native to bauxite mine, Ecotoxicol. Environ. Saf. 107 (2014) 260–268. https://doi.org/10.1016/j.ecoenv.2014.06.009.

[60] C.E. Rodríguez, A. Quesada, E. Rodríguez, Nickel biosorption by Acinetobacter baumannii and Pseudomonas aeruginosa isolated from industrial wastewater, Brazilian J. Microbiol. 37 (2006) 465–467. https://doi.org/10.1590/S1517-83822006000400012.

[61] A. Öztürk, Removal of nickel from aqueous solution by the bacterium Bacillus thuringiensis, J. Hazard. Mater. 147 (2007) 518–523. https://doi.org/10.1016/j.jhazmat.2007.01.047.

[62] F. Veglio, F. Beolchini, A. Gasbarro, Biosorption of toxic metals : an equilibrium study using free cells of Arthrobacter sp ., Process Biochem. 32 (1997) 99–105. https://doi.org/10.1016/S0032-9592(96)00047-7.

[63] The European Parliament and the Council of the European Union, Directive (EU) 2020/2184, EU (revised) Drinking Water Directive. Annex 1. Part B., Off. J. Eur. Communities. 2019 (2020) 35. https://eur-lex.europa.eu/eli/dir/2020/2184/oj.

[64] A.J. Barlow, S. Popescu, K. Artyushkova, O. Scott, N. Sano, J. Hedley, P.J. Cumpson, Chemically specific identification of carbon in XPS imaging using Multivariate Auger Feature Imaging (MAFI), Carbon N. Y. 107 (2016) 190–197. https://doi.org/10.1016/j.carbon.2016.05.073.

[65] T.J. Silhavy, D. Kahne, S. Walker, The Bacterial Cell Envelope, Cold Spring Harb Perspect Biol. 2 (2010) 1–16. https://doi.org/10.1101/cshperspect.a000414.

[66] W. Jiang, A. Saxena, B. Song, B.B. Ward, T.J. Beveridge, S.C.B. Myneni, Elucidation of functional groups on gram-positive and gram-negative bacterial surfaces using infrared spectroscopy, Langmuir. 20 (2004) 11433–11442. https://doi.org/10.1021/la049043+.

[67] N.A. Komandrova, S. V Tomshich, V. V Isakov, L.A. Romanenko, Structure of sulfated O-specific polysaccharide of the marine bacterium Pseudoalteromonas marinoglutinosa KMM 232., Biochemistry. (Mosc). 63 (1998) 1200–1204.

[68] L. Ploux, K. Anselme, A. Dirani, A. Ponche, O. Soppera, V. Roucoules, Opposite Responses of Cells and Bacteria to Micro/Nanopatterned Surfaces Prepared by Pulsed Plasma Polymerization and UV-Irradiation, Langmuir. 25 (2009) 8161–8169. https://doi.org/10.1021/la900457f.

[69] J. Song, P. Peng, Surface Characterization of Aerosol Particles in Guangzhou, China: A Study by XPS, Aerosol Sci. Technol. 43 (2009) 1230–1242. https://doi.org/10.1080/02786820903325394.

[70] J.S. Stevens, A.C. De Luca, M. Pelendritis, G. Terenghi, S. Downes, S.L.M. Schroeder, Quantitative analysis of complex amino acids and RGD peptides by X-ray photoelectron

spectroscopy (XPS), Surf. Interface Anal. 45 (2013) 1238–1246. https://doi.org/10.1002/sia.5261.

[71] P.G. Rouxhet, M.J. Genet, XPS analysis of bio-organic systems, Surf. Interface Anal. 43 (2011) 1453–1470. https://doi.org/10.1002/sia.3831.

[72] V. Arondel, C. Benning, C.R. Somerville, Isolation and functional expression in Escherichia coli of a gene encoding phosphatidylethanolamine methyltransferase (EC 2.1.1.17) from Rhodobacter sphaeroides, J. Biol. Chem. 268 (1993) 16002–16008. https://doi.org/10.1016/s0021-9258(18)82350-x.

[73] P.J. Wilderman, A.I. Vasil, W.E. Martin, R.C. Murphy, M.L. Vasil, Pseudomonas aeruginosa synthesizes phosphatidylcholine by use of the phosphatidylcholine synthase pathway, J. Bacteriol. 184 (2002) 4792–4799. https://doi.org/10.1128/JB.184.17.4792-4799.2002.

[74] S. Furse, D.J. Scott, Three-Dimensional Distribution of Phospholipids in Gram Negative Bacteria, Biochemistry. 55 (2016) 4742–4747. https://doi.org/10.1021/acs.biochem.6b00541.

[75] F.K. Sahrani, M.A. Aziz, Z. Ibrahim, A. Yahya, Surface analysis of marine sulphate-reducing bacteria exopolymers on steel during biocorrosion using X-ray photoelectron spectroscopy, Sains Malaysiana. 37 (2008) 131–135.

[76] K.C. Lemmer, F. Alberge, K.S. Myers, A.C. Dohnalkova, R.E. Schaub, J.D. Lenz, S. Imam, J.P. Dillard, D.R. Noguera, J. Donohue, The NtrYX Two-Component System Regulates the Bacterial Cell Envelope, MBio. 11 (2020) 1–17.

[77] M. Ramstedt, A. Shchukarev, Analysis of bacterial cell surface chemical composition using cryogenic X-ray photoelectron spectroscopy, Methods Mol. Biol. 1440 (2016) 215–223. https://doi.org/10.1007/978-1-4939-3676-2_16.

[78] M. Kjærvik, K. Schwibbert, P. Dietrich, A. Thissen, W.E.S. Unger, Surface characterisation of Escherichia coli under various conditions by near-ambient pressure XPS, Surf. Interface Anal. 50 (2018) 996–1000. https://doi.org/10.1002/sia.6480.

[79] P.G. Adams, L. Lamoureux, K.L. Swingle, H. Mukundan, G.A. Montaño, Lipopolysaccharide-induced dynamic lipid membrane reorganization: Tubules, perforations, and stacks, Biophys. J. 106 (2014) 2395–2407. https://doi.org/10.1016/j.bpj.2014.04.016.

[80] L.A. Clifton, M.W.A. Skoda, A.P. Le Brun, F. Ciesielski, I. Kuzmenko, S.A. Holt, J.H. Lakey, Effect of Divalent Cation Removal on the Structure of Gram-Negative Bacterial Outer Membrane Models, Langmuir. 31 (2015) 404–412. https://doi.org/10.1021/la504407v.

[81] N.A. Amro, L.P. Kotra, K. Wadu-mesthrige, A. Bulychev, S. Mobashery, G. Liu, High-Resolution Atomic Force Microscopy Studies of the Escherichia coli Outer Membrane : Structural Basis for Permeability, Langmuir. 16 (2000) 2789–2796. https://doi.org/10.1021/la991013x.

[82] F.S. Hoseinian, B. Rezai, M. Safari, D. Deglon, E. Kowsari, Separation of nickel and zinc from aqueous solution using triethylenetetramine, Hydrometallurgy. 202 (2021) 105609. https://doi.org/10.1016/j.hydromet.2021.105609.

[83] I.A. Sergeeva, N. V. Sokol, M.S. Ivanova, G.P. Petrova, Y.M. Petrusevich, Molecular mobility in protein solutions containing metal ions with various ionic radii, Moscow Univ. Phys. Bull. 64 (2009) 446–449. https://doi.org/10.3103/S0027134909040201.

[84] H. Chang, K. Gnanasekaran, N.C. Gianneschi, F.M. Geiger, Bacterial Model Membranes Deform (resp. Persist) upon Ni2+ Binding to Inner Core (resp. O-Antigen) of Lipopolysaccharides, J. Phys. Chem. B. 123 (2019) 4258–4270. https://doi.org/10.1021/acs.jpcb.9b02762.

[85] A.M. Salvi, R. Pucciariello, M.R. Guascito, V. Villani, L. Intermite, Characterization of the interface in rubber/silica composite materials, Surf. Interface Anal. 33 (2002) 850–861. https://doi.org/10.1002/sia.1463.

[86] E. Montibon, L. Järnström, M. Lestelius, Characterization of poly(3,4-ethylenedioxythiophene)/poly(styrene sulfonate) (PEDOT:PSS) adsorption on cellulosic materials, Cellulose. 16 (2009) 807–815. https://doi.org/10.1007/s10570-009-9303-3.

[87] P. Pagliara, D. Chirizzi, M.R. Guascito, Chemical characterization of red cells from the black sea urchinArbacia lixulaby X-ray photoelectron spectroscopy, RSC Adv. 11 (2021) 27074–27083. https://doi.org/10.1039/d1ra03156b.

[88] K. Maeda, Y. Okuda, G. Enomoto, S. Watanabe, M. Ikeuchi, Biosynthesis of a sulfated exopolysaccharide, synechan, and bloom formation in the model cyanobacterium Synechocystis sp. strain PCC6803, Elife. 10 (2021) 1–19. https://doi.org/10.7554/eLife.66538.

[89] E.L. Nazarenko, R.J. Crawford, E.P. Ivanova, The structural diversity of carbohydrate

antigens of selected gram-negative marine bacteria, Mar. Drugs. 9 (2011) 1914–1954. https://doi.org/10.3390/md9101914.

[90] C.D. Calvano, F. Italiano, L. Catucci, A. Agostiano, T.R.I. Cataldi, F. Palmisano, M. Trotta, The lipidome of the photosynthetic bacterium Rhodobacter sphaeroides R26 is affected by cobalt and chromate ions stress, BioMetals. 27 (2014) 65–73. https://doi.org/10.1007/s10534-013-9687-2.

[91] B. Tamot, C. Benning, Membrane Lipid Biosynthesis in Purple Bacteria, in: C.N. Hunter, F. Daldal, M.C. Thurnauer, J.T. Beatty (Eds.), Purple Phototrophic Bact. Adv. Photosynth. Respir., Springer, Dordrecht, 2009.

[92] G.F. Lorusso, G. De Stasio, P. Casalbore, D. Mercanti, M.T. Ciotti, A. Cricenti, R. Generosi, P. Perfetti, G. Margaritondo, Photoemission analysis of chemical differences between the membrane and cytoplasm of neuronal cells, J. Phys. D. Appl. Phys. 30 (1997) 1794–1798. https://doi.org/10.1088/0022-3727/30/12/017.

[93] M.C. Biesinger, L.W.M. Lau, A.R. Gerson, R.S.C. Smart, The role of the Auger parameter in XPS studies of nickel metal, halides and oxides, Phys. Chem. Chem. Phys. 14 (2012) 2434–2442. https://doi.org/10.1039/C2CP22419D.

[94] Y. Ávila-Torres, L. Huerta, N. Barba-Behrens, XPS-characterization of heterometallic coordination compounds with optically active ligands, J. Chem. 2013 (2013) Article ID 370637. https://doi.org/10.1155/2013/370637.

[95] C.D. Wagner, L.H. Gale, R.H. Raymond, Two-dimensional chemical state plots: a standardized data set for use in identifying chemical states by x-ray photoelectron

spectroscopy, Anal. Chem. 51 (1979) 466–482. https://doi.org/10.1021/ac50040a005.

[96] X. Tan, M. Fang, C. Chen, S. Yu, X. Wang, Counterion effects of nickel and sodium dodecylbenzene sulfonate adsorption to multiwalled carbon nanotubes in aqueous solution, Carbon N. Y. 46 (2008) 1741–1750. https://doi.org/10.1016/j.carbon.2008.07.023.

HIGHLIGHTS

- Ni^{2+} extracellular uptake by *Rhodobacter sphaeroides* follows the Langmuir model.
- Ni^{2+} fully displace alkali metal ions while Ca^{2+} and Mg^{2+} remain bound to the surface.
- Single component XPS analysis enables assessing Ni^{2+}-induced surface modifications.
- Ni^{2+} binding causes stacking and/or packing of lipopolysaccharide moieties.

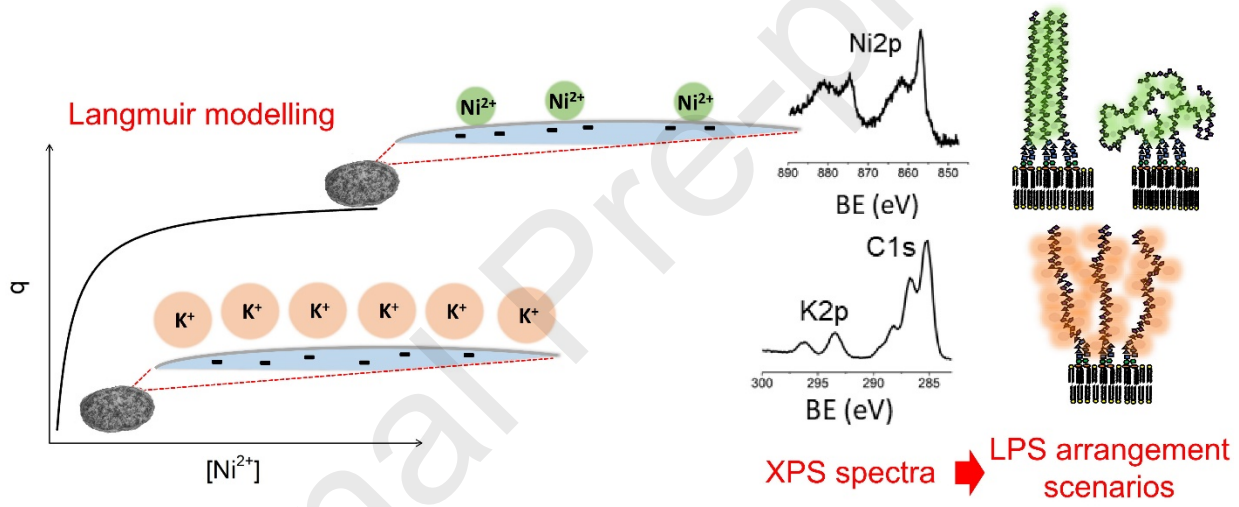

Declaration of interests

☒ The authors declare that they have no known competing financial interests or personal relationships that could have appeared to influence the work reported in this paper.

☐The authors declare the following financial interests/personal relationships which may be considered as potential competing interests:

Sample CRediT author statement

Daniela Chirizzi: Investigation, Formal Analysis, Visualization. **Disma Mastrogiacomo**: Investigation, Visualization. **Paola Semeraro**: Investigation, Visualization, Writing - Review & Editing. **Francesco Milano**: Software, Writing - Review & Editing. **Anna Rita De Bartolomeo**: Investigation, Formal analysis. **Massimo Trotta**: Conceptualization, Methodology, Resources, Supervision, Project Administration. **Ludovico Valli**: Writing - Review & Editing, Supervision, Project Administration. **Livia Giotta**: Conceptualization, Methodology, Formal Analysis, Validation, Visualization, Investigation, Data Curation, Writing - Original Draft, Writing - Review & Editing, Supervision. **Maria Rachele Guascito**: Conceptualization, Methodology, Formal Analysis, Validation, Investigation, Data Curation, Writing - Original Draft, Supervision.